Vimentin-Binding Aptamer Motifs for Ovarian Cancer

Subjects: Biochemistry & Molecular Biology

Contributor: Hongyu Wang

The application of aptamers in biomedicine is emerging as an essential technology in the field of cancer research. As small single-stranded DNA or RNA ligands with high specificity and low immunogenicity for their targets, aptamers provide many advantages in cancer therapeutics over protein-based molecules, such as antibodies. Vimentin is an intermediate filament protein that is overexpressed in endothelial cells of cancerous tissue. High expression levels of vimentin have been associated with increased capacity for migration and invasion of the tumor cells. We have selected and identified thioated aptamers with high specificity for vimentin using human ovarian cancer tissues. Tentative binding motifs were chosen for two vimentin aptamers based on predicted secondary structures. Each of these shorter, tentative binding motifs was synthesized, purified, and characterized via cell binding assays. Two vimentin binding motifs with high fidelity binding were selected and further characterized via cell and tissue binding assays, as well as flow cytometric analysis. The equilibrium binding constants of these small thioated aptamer constructs were also determined. Future applications for the vimentin binding aptamer motifs include conjugation of the aptamers to synthetic dyes for use in targeted imaging and therapy, and ultimately more detailed and precise monitoring of treatment response and tumor progression in ovarian pathology.

Keywords: aptamer ; binding motifs ; ovarian cancer

1. Introduction

Aptamers are single-stranded nucleic acids with defined tertiary structures for selective binding to target molecules by utilizing complementary shape interactions. The secondary structures of aptamers can be predicted from their sequences [1]. Many programs have been developed to identify and study aptamer binding motifs, including AptaTRACE [2] for identifying sequence-structure binding motifs in high-throughput systematic evolution of ligands by exponential enrichment (HT-SELEX) data. Aptamotif [3] and APTANI [4] also identified sequence-structure motifs in SELEX-derived aptamers using an ensemble-based approach. As only a small fraction of the sequence is involved in direct contact with the target, aptamer truncation can be used to find the minimum sequence while maintaining selective binding activity. Ultimately, aptamer truncation will help to reduce the material cost of aptamer synthesis, enable material quality assurance and prevent unexpected toxicity [5][6][7][8]. Many studies have demonstrated effective aptamer truncations in different ways. Truncations on the stem-loop regions showed a significant increase in the binding affinity for the VEGF-165 [9]. Aptamer acquisition from a random region has shown successful identification of 15 nt [10] or 20 nt [11] aptamers. Moreover, a 14 nucleotides aptamer was reported as the smallest functional unit of the transferrin receptor aptamer with enhanced binding affinity to the transferrin receptor [12].

Vimentin is an extracellular matrix protein that is part of the intermediate filament protein family [13]. Overexpression of vimentin may be associated with increased metastatic capacity through the epithelial to mesenchymal transformation (EMT) of ovarian tumor cells [14]. Studies have shown that increased expression of vimentin correlates to decreased survival rate in a variety of cancers such as colorectal, cervical, breast, gastric, and non-small cell lung cancers, to name a few [15][16][17]. There are limited studies, however, exploring the relationship between vimentin expression and ovarian tumor prognosis. A recent study by Szubert et al. [18] showed a prolonged overall survival rate with an increased rate of vimentin expression in the ovarian tumor cells. While this relationship is contrary to that seen in other tumor pathologies, it remains evident that a relationship exists between vimentin and overall tumor prognosis, and a marker for vimentin would serve as an invaluable tool in assessing tumor prognosis, as well as potentially serving as a marker for targeted molecular imaging. Currently, there are aptamers against vimentin for isolation of circulating tumor cells undergoing epithelial mesenchymal transition [19]. Zamay et al. used aptamer NAS-24 which binds to vimentin for intracellular targeting of mouse ascites adenocarcinoma cells in vitro and in vivo [20]. We have identified two phosphorothioated aptamers, thioaptamers, V3 and V5 that have high affinity and specificity binding to vimentin through our innovative morphology-based tissue aptamer selection (Morph-X-Select) method [21]. The secondary structure prediction suggests that those aptamers would form 3–4 stem-loop structures. The originally selected V3 and V5 aptamers were 74-mer in length and

had high affinities to vimentin (Kd = 42.46 nM, Kd = 95.22 nM, respectively). As the recognition-based binding activity between the DNA aptamer and vimentin protein is dependent on the secondary structure of the vimentin aptamer, we further analyzed predictive secondary structures of the aptamers to identify sequence features and patterns by Mfold [1], and conducted a few truncations on the stem-loop regions to achieve improved binding affinity with the truncated aptamers.

2. Analysis on Results

2.1. Identification of Potential Aptamer Binding Motifs

To improve upon the binding affinity of the vimentin binding aptamers that were identified in previous work by Wang et al. [21], the secondary structures of two vimentin binding aptamers (V3 and V5) were analyzed by Mfold to estimate short binding motifs. As the stems and loops structures are central to target molecule recognition, we conducted aptamer truncation on the stem-loop regions and generated seven truncated motifs. The selected secondary structures of V3 and V5 with their respective tentative binding motifs are shown in **Figure 1**. After identifying the binding motif sequences, we synthesized those binding motifs individually with modification of monothioated phosphates on their 3′ sides of adenines.

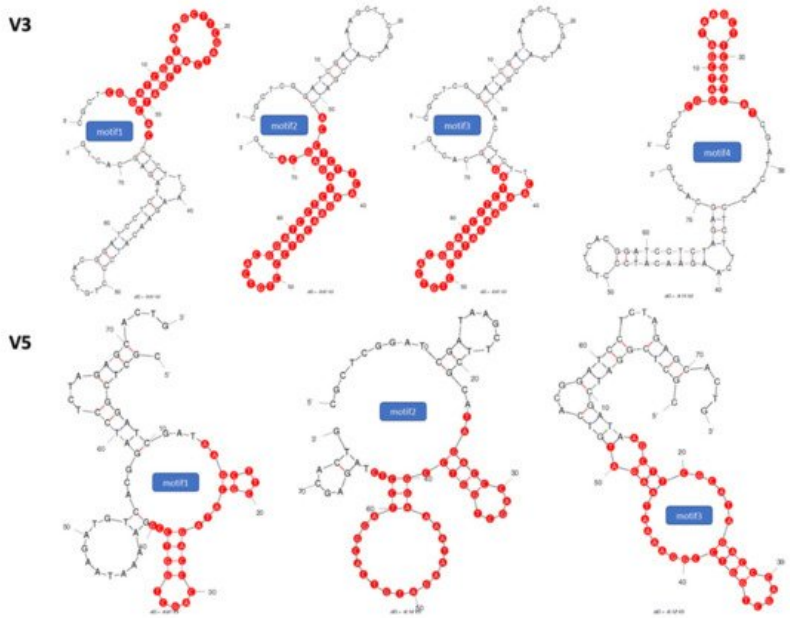

Figure 1. Secondary structures of selected (**V3**) and (**V5**) thio-aptamers. Proposed binding motifs are shown in red.

2.2. Screening of Synthesized Aptamer Motifs

After synthesis and purification of all seven aptamer motifs, the binding affinity of each motif was assessed using the ovarian tumor IGROV cell line. Vimentin expression of IGROV cells was evaluated and confirmed using anti-human vimentin antibody before screening the motifs binding affinity (**Figure 2**C).

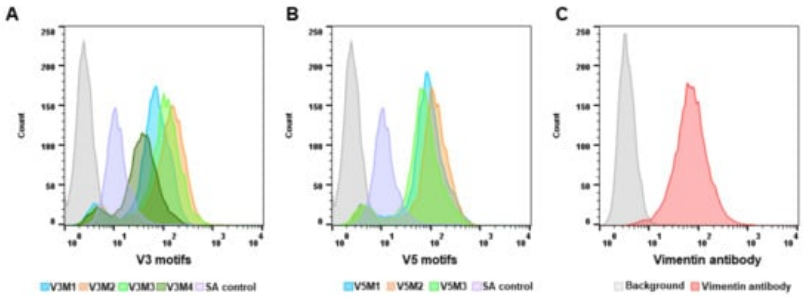

Figure 2. Screening of synthesized aptamer motifs. Synthesized biotinylated motifs of V3 and V5 were incubated with IGROV cells. Fluorescein isothiocyanate (FITC) conjugated streptavidin is used to detect biotinylated motifs. The binding affinity of the aptamer motifs was assessed based on the fluorescence intensity using flow cytometry. Histogram graphs demonstrated the fluorescence intensity of V3 aptamer motifs (**A**), and V5 aptamer motifs (**B**) binding to IGROV cells. Vimentin expression was evaluated and confirmed using an anti-human vimentin antibody before screening the binding affinity of motifs (**C**). A scrambled aptamer was used as a control.

Afterward, cells were incubated with the vimentin-aptamer motifs and their binding affinity was assessed using flow cytometry. Based on the fluorescence intensity of each motif binding to the cells, the V3 aptamer motif 2 (V3M2) (**Figure 2**A) and the V5 aptamer motif 2 (V5M2) (**Figure 2**B) that have the highest fluorescent intensity of each group were selected for future experimentations and their sequences are listed in **Table 1**.

Table 1. Selected short binding motifs.

Name	Sequences
V3M2 (40 mer)	**5'-ACCTCTTCAAGAACATCCCTGTCACGGATCCTCTAGAGCA-3'**
V5M2 (41 mer)	**5'-TAGACCCAGCTGGTCCGGAAAATAAGATGTCACGGATCCTC-3'**
Scrambled Control (40 mer)	**5'-CCCACTTATCGTCCCTTAATGAGTTTACTCGCACACCGGA-3'**

2.3. Binding Affinity of Selected V3M2 and V5M2

To quantitatively evaluate the binding affinity of the selected V3M2 and V5M2, filter-binding assays were performed with vimentin protein. The spot intensities of chemiluminescent signals were measured to establish saturation binding curves as shown in **Figure 3**A, lower panel. The equilibrium dissociation constants, Kd, were derived from these curves and are determined as V3M2 = 18.94 nM and V5M2 = 47.35 nM, respectively. Representative spot image demonstrated that biotinylated V3M2 and V5M2 bind with vimentin protein retained on the nitrocellulose membrane, while non-binding aptamers stained on nylon membrane (**Figure 3**B). Furthermore, the binding affinity of the short motifs V3M2 and V5M2 to vimentin protein was better than the binding affinity of the original V3 and V5 thioaptamers (Kd = 42.46 nM, Kd = 95.22 nM, respectively) (**Figure 3**A, upper panel).

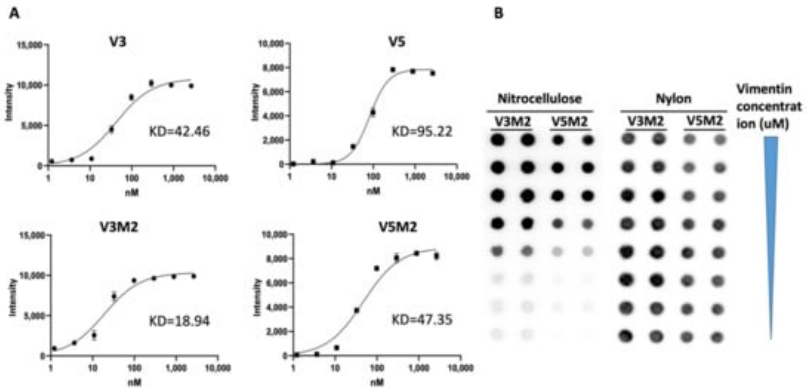

Figure 3. The binding affinity of V3, V5, selected motifs and their equilibrium dissociation constant. Filter-binding assays were performed with the biotinylated V3, V5, V3M2, V5M2 thioaptamers and purified vimentin protein. Chemiluminescent detection of spot intensities on the nitrocellulose membranes was used to quantitate the thio-aptamer binding affinity. (**A**) Saturation binding curves were generated and the equilibrium dissociation constants, Kd, were calculated from the equation Y = Bmax × X/(Kd + X), assuming a single binding site. Bmax represents the maximum binding capacity of aptamer bound to vimentin protein. X is the protein concentrations and Y is the calculated spot intensity. (**B**) Representative spot image of biotinylated V3M2 and V5M2 binding with vimentin protein retained on the nitrocellulose membrane. Non-binding motifs stained on a nylon membrane.

2.4. Dose Response of V3M2 and V5M2

To quantitatively evaluate the binding affinity of selected V3M2 and V5M2 further, vimentin expressing IGROV cells were incubated with biotin conjugates motifs at various concentrations (31, 125, 500 nM for V3M2, and 41, 166, 666 nM for V5M2), followed by streptavidin-FITC staining. The binding affinity of V3M2 and V5M2 at various concentrations was determined by mean fluorescence intensity using flow cytometry. Histograms of the fluorescence intensity above the background for V3M2 and V5M2 are shown in **Figure 4**A,B, respectively. These data demonstrated that the binding of both V3M2 and V5M2 to IGROV cells occurs in a dose-dependent manner. Moreover, at the same aptamer concentration, V3M2 showed better binding with higher fluorescence intensity than the binding of V5M2 to IGROV cells. This result is also consistent with the results of filter binding analysis in **Figure 3**.

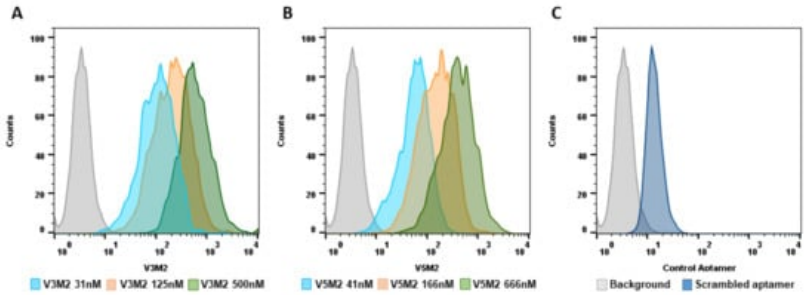

Figure 4. Dose-dependent binding of selected motifs. Biotin conjugated V3M2 and V5M2 were incubated with vimentin-expressing IGROV cells at various concentrations and followed by streptavidin-FITC staining. Their binding affinity was analyzed by flow cytometry. Histograms presenting the fluorescence intensity above the background were shown for V3M2 (**A**) and V5M2 (**B**). A scrambled control aptamer with non-specific and low binding affinity is also assessed (**C**).

2.5. Validation of Selected Motifs with Human Cells

To evaluate the binding efficiency and specificity, the performance of V3M2 and V5M2 binding to IGROV cells were compared with anti-human vimentin antibodies. Vimentin expressing IGROV cells were incubated with either V3M2, V5M2, or anti-human vimentin antibodies. The binding proficiency of V3M2, V5M2, or vimentin antibody was examined by fluorescence microscopy and quantified by normalizing fluorescence intensity of pixel per area (intensity of motif/intensity of DAPI) and are presented as a bar graph with mean ± SE of three replicates (**Figure 5**).

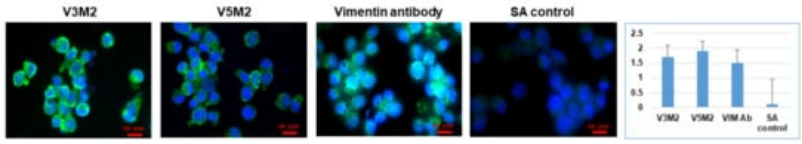

Figure 5. Validating specific binding of selected motifs with the human cell line. Vimentin-expressing IGROV cells were incubated with biotinylated V3M2, V5M2, anti-human vimentin antibody (VIM Ab) or scrambled control (SA) aptamer. Fluorescein isothiocyanate (FITC) conjugated streptavidin was used to detect biotinylated aptamers. The binding proficiencies were determined by fluorescence intensity using fluorescence microscopy. Fluorescence intensity is quantified by normalizing the fluorescence intensity of pixel per area (intensity of motif/intensity of DAPI) and presented as a bar graph with mean ± SE of three replicates. Hoechst 33342 was used to stain the cell nuclei (blue).

Both V3M2 and V5M2 demonstrated similar binding affinity to vimentin expressing IGROV cells, compared to the binding intensity of vimentin antibody. Specific bindings of V3M2 and V5M2 were confirmed by minimal fluorescence detection from scrambled control aptamer incubated with IGROV cells.

2.6. Validation of Selected Motifs with Human Ovarian Tumor

After confirming aptamer binding in IGROV cells, the binding of the aptamers was further assessed in human ovarian tissue samples. Each aptamer was evaluated in both normal ovarian tissue samples and ovarian tumor tissue samples as displayed in **Figure 6**. The top row represented the strong binding of V3M2, V5M2 and anti-vimentin antibodies in human ovarian tumor tissue, while the bottom panel represented the weak binding of V3M2, V5M2 and anti-vimentin antibody in normal human ovarian tissue. All aptamers in this assay were used at a concentration of 250 nM. Images are representative of three samples of ovarian tumor or normal ovarian tissue. Fluorescence intensity is quantified by normalizing the fluorescence intensity of pixel per area (intensity of motif/intensity of DAPI) and presented as a bar graph with mean ± SE of three replicates. This observation is consistent with other studies that reported increased vimentin expression in various tumor cell lines and tissues including ovarian cancers [18], endometrial cancer [22] and many other tumors [23].

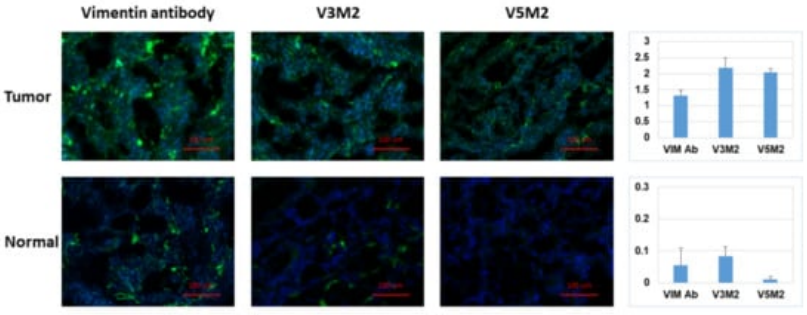

Figure 6. Detection of vimentin expression in human ovarian tumor tissue. Tissue sections of human ovarian tumor or normal ovarian tissue were incubated with biotinylated V3M2 or V5M2 at a concentration of 250 nM, followed by streptavidin-FITC to detect their binding affinity. Anti-human vimentin antibody was also used as a positive control for both ovarian tumor tissue and normal ovarian tissue. Images are representative of three samples of ovarian tumor or normal ovarian tissue. Fluorescence intensity is quantified by normalizing the fluorescence intensity of pixel per area (intensity of motif/intensity of DAPI) and presented as a bar graph with mean ± SE of three replicates. Hoechst 33342 was used to stain the cell nuclei (blue).

3. Current Insights

Aptamer truncation is an important approach to lower the material cost of synthesis, improve on-target binding, and reduce non-target interactions of an aptamer. Based on secondary structure prediction, one can identify potential aptamer binding motifs as a way of truncating the sequence while maintaining selective binding activity. As the stems and loops structures are central to target molecule recognition, truncation on the stem-loop regions has demonstrated improved accessibility of targets to the aptamer, resulting in stronger aptamer-target binding [9]. Therefore, we conducted aptamer truncation on the stem-loop regions based on analysis of their predicted secondary structures of our identified V3 and V5 aptamers, and generated seven truncated motifs. The shortened motifs with fewer thiophosphate modifications can also reduce the non-specific binding against both target and non-target proteins compared with the normal phosphodiester bond [24]. By screening the binding affinity of the seven truncated motifs with vimentin expressing IGROV cells, we selected V3M2 and V5M2 based on their highest fluorescence intensity among truncations of V3 and V5 groups, respectively. When examining the sequences and secondary structures of the V2M2 and V5M2, we found both of them are the longest sequence in their truncated groups. Considering the stem-loop structures of V3M2 and V5M2, it is possible that the longer sequence contributes to the bigger loop and leads to better binding to the target protein. In fact, Armstrong et al. reported that the highest binding affinities were observed with full exposure of the aptamer sequence in the loop, while duplex formation reduced binding affinity most likely due to the thermodynamics of DNA base pairing [25]. This implies that the optimal motif selection might be to choose those motifs that have a long sequence size of the hairpin loop to accommodate both stem interactions and loop stability.

References

1. Zuker, M. Mfold web server for nucleic acid folding and hybridization prediction. Nucleic Acids Res. 2003, 31, 3406–3415.
2. Dao, P.; Hoinka, J.; Takahashi, M.; Zhou, J.; Ho, M.; Wang, Y.; Costa, F.; Rossi, J.J.; Backofen, R.; Burnett, J.; et al. AptaTRACE Elucidates RNA Sequence-Structure Motifs from Selection Trends in HT-SELEX Experiments. Cell Syst. 2016, 3, 62–70.
3. Hoinka, J.; Zotenko, E.; Friedman, A.; Sauna, Z.E.; Przytycka, T.M. Identification of sequence-structure RNA binding motifs for SELEX-derived aptamers. Bioinformatics 2012, 28, i215–i223.
4. Caroli, J.; Taccioli, C.; De La Fuente, A.; Serafini, P.; Bicciato, S. APTANI: A computational tool to select aptamers through sequence-structure motif analysis of HT-SELEX data. Bioinformatics 2015, 32, 161–164.
5. Adachi, T.; Nakamura, Y. Aptamers: A Review of Their Chemical Properties and Modifications for Therapeutic Application. Molecules 2019, 24, 4229.
6. Henry, S.P.; Giclas, P.C.; Leeds, J.; Pangburn, M.; Auletta, C.; Levin, A.A.; Kornbrust, D.J. Activation of the alternative pathway of complement by a phosphorothioate oligonucleotide: Potential mechanism of action. J. Pharmacol. Exp. Ther. 1997, 281, 810–816.
7. Qi, C.; Bing, T.; Mei, H.; Yang, X.; Liu, X.; Shangguan, D. G-quadruplex DNA aptamers for zeatin recognizing. Biosens. Bioelectron. 2013, 41, 157–162.
8. Mei, H.; Bing, T.; Yang, X.; Qi, C.; Chang, T.; Liu, X.; Cao, Z.; Shangguan, D. Functional-group specific aptamers indirectly recognizing compounds with alkyl amino group. Anal. Chem. 2012, 84, 7323–7329.
9. Kaur, H.; Yung, L.Y. Probing high affinity sequences of DNA aptamer against VEGF165. PLoS ONE 2012, 7, e31196.
10. Kupakuwana, G.V.; Crill, J.E., 2nd; McPike, M.P.; Borer, P.N. Acyclic identification of aptamers for human alpha-thrombin using over-represented libraries and deep sequencing. PLoS ONE 2011, 6, e19395.
11. Thiel, W.H.; Bair, T.; Thiel, K.W.; Dassie, J.P.; Rockey, W.M.; Howell, C.A.; Liu, X.Y.; Dupuy, A.J.; Huang, L.; Owczarzy, R.; et al. Nucleotide bias observed with a short SELEX RNA aptamer library. Nucleic Acid Ther. 2011, 21, 253–263.

12. Macdonald, J.; Houghton, P.; Xiang, D.; Duan, W.; Shigdar, S. Truncation and Mutation of a Transferrin Receptor Aptamer Enhances Binding Affinity. Nucleic Acid Ther. 2016, 26, 348–354.
13. Eriksson, J.E.; Dechat, T.; Grin, B.; Helfand, B.; Mendez, M.; Pallari, H.M.; Goldman, R.D. Introducing intermediate filaments: From discovery to disease. J. Clin. Investig. 2009, 119, 1763–1771.
14. Zhao, L.; Zhang, P.; Su, X.-J.; Zhang, B. The ubiquitin ligase TRIM56 inhibits ovarian cancer progression by targeting vimentin. J. Cell. Physiol. 2018, 233, 2420–2425.
15. Du, L.; Li, J.; Lei, L.; He, H.; Chen, E.; Dong, J.; Yang, J. High Vimentin Expression Predicts a Poor Prognosis and Progression in Colorectal Cancer: A Study with Meta-Analysis and TCGA Database. BioMed Res. Int. 2018, 2018, 6387810.
16. Yin, S.; Chen, F.F.; Yang, G.F. Vimentin immunohistochemical expression as a prognostic factor in gastric cancer: A meta-analysis. Pathol. Res. Pract. 2018, 214, 1376–1380.
17. Zou, S.S.H.; Fan, L.; Xiao, X.; Gong, L.; Zhu, J.; Chen, X. Prognostic indicators in patients with early stage endometrioid adenocarcinoma: A retrospective case-control study of 523 patients. Int. J. Clin. Exp. Med. 2017, 10, 3699–3705.
18. Szubert, S.; Koper, K.; Dutsch-Wicherek, M.M.; Jozwicki, W. High tumor cell vimentin expression indicates prolonged survival in patients with ovarian malignant tumors. Ginekol. Pol. 2019, 90, 11–19.
19. Zheng, Y.; Zhang, J.; Huang, M.; Wang, T.; Qu, X.; Wu, L.; Song, J.; Wang, W.; Song, Y.; Yang, C. Selection of Aptamers Against Vimentin for Isolation and Release of Circulating Tumor Cells Undergoing Epithelial Mesenchymal Transition. Anal. Chem. 2020, 92, 5178–5184.
20. Zamay, T.N.; Kolovskaya, O.S.; Glazyrin, Y.E.; Zamay, G.S.; Kuznetsova, S.A.; Spivak, E.A.; Wehbe, M.; Savitskaya, A.G.; Zubkova, O.A.; Kadkina, A.; et al. DNA-aptamer targeting vimentin for tumor therapy in vivo. Nucleic Acid Ther. 2014, 24, 160–170.
21. Wang, H.; Li, X.; Volk, D.E.; Lokesh, G.L.-R.; Elizondo-Riojas†, M.-A.; Li, L.; Nick, A.M.; Sood, A.K.; Rosenblatt, K.P.; Gorenstein, D.G. Morph-X-Select: Morphology-based tissue aptamer selection for ovarian cancer biomarker discovery. Biotechniques 2016, 61, 249–259.
22. Coppola, D.; Fu, L.; Nicosia, S.V.; Kounelis, S.; Jones, M. Prognostic significance of p53, bcl-2, vimentin, and S100 protein-positive Langerhans cells in endometrial carcinoma. Hum. Pathol. 1998, 29, 455–462.
23. Satelli, A.; Li, S. Vimentin in cancer and its potential as a molecular target for cancer therapy. Cell. Mol. Life Sci. 2011, 68, 3033–3046.
24. Gaus, H.J.; Gupta, R.; Chappell, A.E.; Østergaard, M.E.; Swayze, E.E.; Seth, P.P. Characterization of the interactions of chemically-modified therapeutic nucleic acids with plasma proteins using a fluorescence polarization assay. Nucleic Acids Res. 2019, 47, 1110–1122.
25. Armstrong, R.E.; Strouse, G.F. Rationally manipulating aptamer binding affinities in a stem-loop molecular beacon. Bioconjug. Chem. 2014, 25, 1769–1776.
